PAPER

Check for updates

Li-ion diffusion in Li intercalated graphite C6Li and C12Li probed by μ+SR

Izumi Umegaki, [ID] *[a] Shigehiro Kawauchi,[a] Hiroshi Sawada,[a] Hiroshi Nozaki,[a] Yuki Higuchi,[a] Kazutoshi Miwa,[a] Yasuhito Kondo,[a] Martin Månsson,[b] Mark Telling,[c] Fiona C. Coomer,[c] Stephen P. Cottrell,[c] Tsuyoshi Sasaki,[a] Tetsuro Kobayashi[a] and Jun Sugiyama[a]

In order to study a diffusive behavior of Li^+ in Li intercalated graphites, we have measured muon spin relaxation (μ^+SR) spectra for C_6Li and $C_{12}Li$ synthesized with an electrochemical reaction between Li and graphite in a Li-ion battery. For both compounds, it was found that Li^+ ions start to diffuse above 230 K and the diffusive behavior obeys a thermal activation process. The activation energy (E_a) for C_6Li is obtained as 270(5) meV, while E_a = 170(20) meV for $C_{12}Li$. Assuming a jump diffusion of Li^+ in the Li layer of C_6Li and $C_{12}Li$, a self-diffusion coefficient D_{Li} at 310 K was estimated as $7.6(3) \times 10^{-11}$ ($cm^2 s^{-1}$) in C_6Li and $14.6(4) \times 10^{-11}$ ($cm^2 s^{-1}$) in $C_{12}Li$.

1 Introduction

1.1 Li intercalated graphites

Graphite[1] is the most common material for Li-ion batteries,[2] because of its high rechargeable capacity, low voltage, high cycle performance, and relatively low cost. During a charge (discharge) reaction in the Li-ion batteries, Li^+ ions are intercalated into (deintercalated from) graphite.

Fig. 1 illustrates schematic structures of three Li intercalated graphites (LIG), namely, graphite, $C_{12}Li$, and C_6Li, where C_6Li corresponds to the structure for a fully charged state. The structure of LIG is an alternating stack along the c-axis with a graphene layer (G) and Li layer (L). That is, $C_{12}Li$ is represented as GGLGGL, whereas C_6Li as LGLG. Such a structure is usually called a stage structure and the stage number (n) is defined as the number of graphene layers between two adjacent Li layers.

In the c plane of $C_{12}Li$, and C_6Li, one third of the centers of six-member carbon rings are occupied by Li ions, leading to the formation of a $\sqrt{3} \times \sqrt{3}$ super lattice structure [Fig. 1(d) and (f)]. The structural parameters of graphite, $C_{12}Li$, and C_6Li are summarized in Table 1. Note that, although the c-axis length changes with n, the a-axis length is independent of n for $C_{12}Li$, and C_6Li.

1.2 Motivation for measuring Li diffusion

Li diffusion in solids is one of the most important parameters to determine the charge and discharge rate of the Li-ion

[a] Toyota Central R&D Laboratories, Inc., Nagakute, Aichi, 480-1192, Japan. E-mail: umegaki@mosk.tytlabs.co.jp; Fax: +81-561-63-6448; Tel: +81-561-71-8111

[b] Department of Materials and Nanophysics, KTH Royal Institute of Technology, Electrum 229, SE-16440 Kista, Sweden

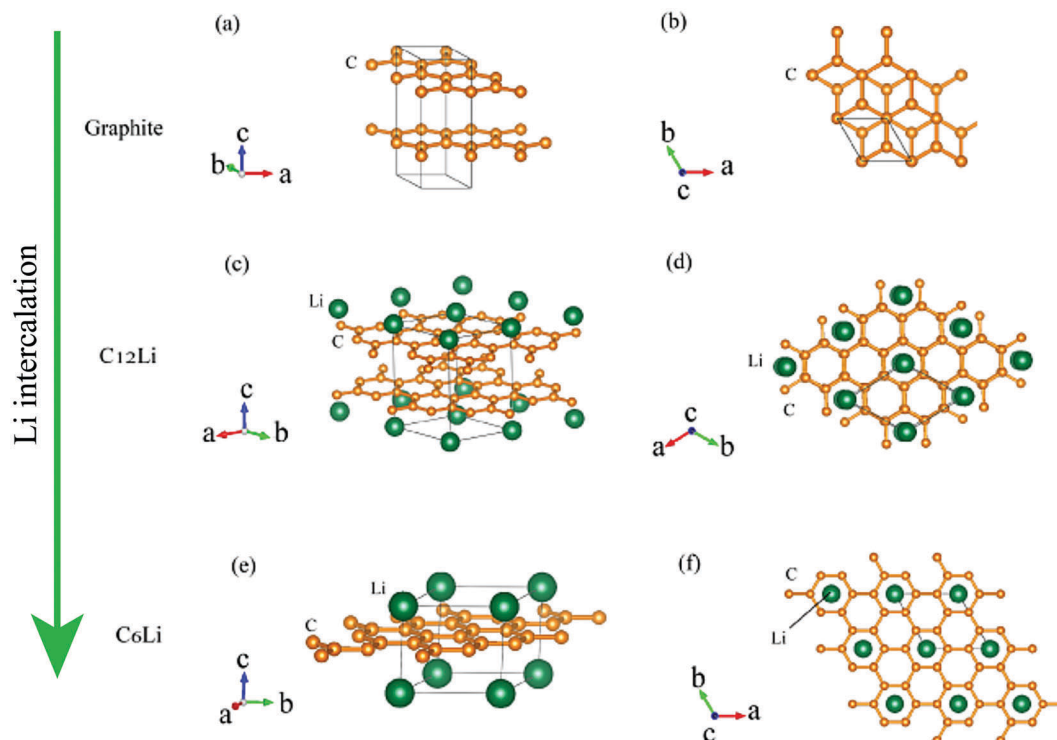*[c] ISIS Muon Facility, Rutherford Appleton Laboratory, Didcot, Oxfordshire, OX11 0QX, UK*

batteries. Particularly, we have the following two motivations to measure a diffusion coefficient of Li^+ (D_{Li}) in LIG with muon spin relaxation (μ^+SR).

- Intrinsic D_{Li}

Since Li^+ ions are thought to diffuse very rapidly in the LIG lattice due to the layered structure, many researchers have believed that D_{Li} in LIG is larger than that in the positive electrode materials, such as, Li_xCoO_2,[6] Li_xNiO_2,[7] Li_xFePO_4,[8,9] and $(Li_xCo_{1/3}Ni_{1/3}Mn_{1/3})O_2$.[10] However, according to recent Li-NMR measurements on C_6Li, D_{Li} was reported as 3.8×10^{-11} $cm^2 s^{-1}$ ($= 3.8 \times 10^{-4}$ $m^2 s^{-1}$) at 314 K,[11] which ranges roughly in the same order of D_{Li} in Li_xCoO_2. Although there are many reports on D_{Li} in LIG with electrochemical techniques, which provide property in a device or setup, not property intrinsic for LIG itself. It is very difficult to determine the intrinsic D_{Li} with such techniques due to the lack of information on the correct reaction surface area of the LIG electrode in a liquid electrolyte.[10]

On the contrary, μ^+SR is known to provide a very reasonable D_{Li} for several positive electrode materials.[6–10,12,13] This is because μ^+SR "sees" the change in local magnetic environments due to Li diffusion. As a result, we obtain intrinsic D_{Li} in battery materials. Therefore, we have attempted to investigate a diffusive behavior in LIG with μ^+SR.

- *In operando* measurements in the near future

For the present Li-NMR and μ^+SR measurements, battery materials have to be removed from a battery. However, it is highly preferable to observe the diffusive behavior both in positive electrode and anode as a function of the state of charge (SOC). In other words, we need to measure D_{Li} of battery materials in a living battery in an *in operando* manner.[14,15]

Fortunately, the range of the surface muons, which is the most common muon beam in the muon facilities in the world,

19058 | *Phys. Chem. Chem. Phys.*, 2017, **19**, 19058–19066

This journal is © the Owner Societies 2017

Fig. 1 The crystal structure of (a) and (b) graphite, (c) and (d) $C_{12}Li$, and (e) and (f) C_6Li. (b, d, and f) Show a c-axis view of graphite, $C_{12}Li$, and C_6Li, in which Li locates at the center of six-member rings of carbon. The structures were drawn with VESTA.[3]

Table 1 Structural parameters of Li-intercalated graphites

Compound	Stage	Li order	a (Å)	c (Å)
Graphite[4]	—	—	2.46	6.71
$C_{12}Li$[5]	2	$\sqrt{3} \times \sqrt{3}$	4.29	7.02
C_6Li[5]	1	$\sqrt{3} \times \sqrt{3}$	4.29	3.737

is about 150 mg cm^{-2} (= 1.5 kg m^{-2}). Based on a simple Montecarlo simulation,[16] such surface muons stop in a Li_xCoO_2 electrode with 50 μm thickness through an aluminum plate with 630 μm thickness. This means that we can measure D_{Li} of electrode materials in functioning Li-ion batteries in the near future. For such a purpose, we also have to initiate measurement of D_{Li} in negative electrode materials with μ$^+$SR.

Here, we report the μ$^+$SR results on LIG with two different stage structures, that is, $C_{12}Li$, and C_6Li. Particularly, in order to apply to *in operando* measurements in the near future, we have not used pure LIG material but an negative electrode sheet, for which the mixture of LIG and binder (PVdF) is coated on the Cu foil.

2 Experimental

2.1 Fabrication of test cell

In order to prepare C_6Li ($C_{12}Li$), a graphite half (pouch) cell was fabricated with graphite and Li metal as electrodes. At first, a graphite electrode sheet was prepared by casting the slurry, which consists of 95% of artificial graphite (OMAC, Osaka Gas Chemicals Co., Ltd) and 5 wt% of polyvinylidene fluoride in the

N-methyl 2-pyrrolidone solvent, onto a Cu foil with 10 μm thickness. Then, the electrode sheet was dried and pressed so as to reduce the thickness down to 82 μm and increase the areal density up to 9.89 mg cm^{-2}. And then, the pouch cell was assembled in an Ar-filled glove box. The electrolyte was 1 M $LiPF_6$ dissolved in ethylene carbonate (EC) and diethyl carbonate (DEC) (3/7 v/v) solution.

2.2 Electrochemical preparation

The pouch cell was charged and discharged under a constant current condition at 0.04 C in the voltage (E) range between 0 and 1500 mV. Note that 1 C means the charge (discharge) rate from empty (full) to full (empty) with one hour. The current and the current density were 3 mA and 0.2 mA cm^{-2}. Electrochemical measurements were performed at 25 °C by an electrochemical analyzer (ACD-01, Aska Electronic co., Ltd) to determine the initial capacity. Fig. 2(a) shows initial charge and discharge cycles, where Li$^+$ ions are intercalated into the graphite when E decreases, while Li$^+$ ions are deintercalated from the graphite when E increases. After the initial two cycles, the pouch cell was discharged down to $E = 88$ mV [Fig. 2(b)], which is estimated as E for $C_{12}Li$ in Open Circuit Voltage measurements. Then, E was kept at 88 mV to obtain a homogeneous $C_{12}Li$ sheet.

For C_6Li, after the initial one cycle between 1500 mV and 5 mV (Fig. 3), the test cell was discharged to $E = 5$ mV and wrapped with an aluminum foil so as to achieve $E = 0$ V and kept for a week. The color of the obtained C_6Li was typical golden yellow [Fig. 4(a)] and E was lower than 1 mV. From now on, we call the charged electrode C_6Li and/or $C_{12}Li$ sheet.
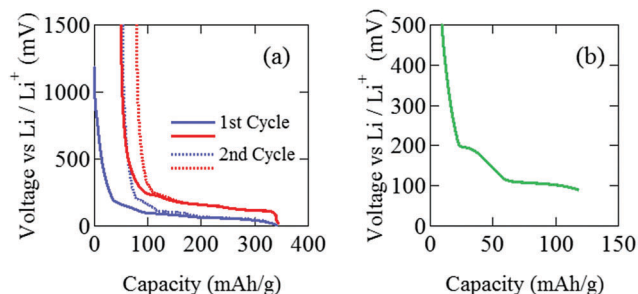
This journal is © the Owner Societies 2017

Phys. Chem. Chem. Phys., 2017, **19**, 19058–19066 | 19059

Fig. 2 The variation of voltage (E) of a graphite‖Li half pouch cell. (a) Li$^+$ ions are intercalated into (deintercalated from) graphite as E decreases (increases). After the initial two cycles, (b) the cell was discharged down to $E = 88$ mV, and then kept at $E = 88$ mV for 10 hours to obtain a homogeneous sample.
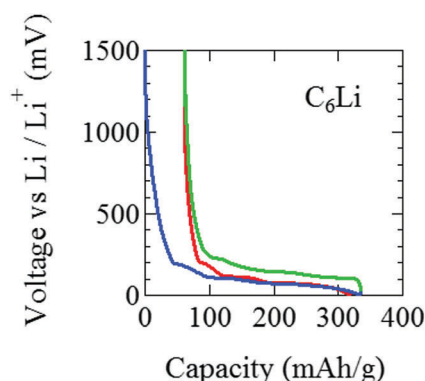

Fig. 3 The variation of voltage (E) of a graphite‖Li half pouch cell. Li$^+$ ions are intercalated into (deintercalated from) graphite as E decreases (increases). After the initial cycle, the cell was discharged down to $E = 5$ mV, and then wrapped with aluminum foils for a week to obtain a homogeneous sample.

The composition of C_6Li and $C_{12}Li$ was confirmed by the ICP-OES technique (CIROS 120EOP, Rigaku).

2.3 μ$^+$SR

The C_6Li and $C_{12}Li$ sheets were removed from the pouch cells, rinsed with dimethyl carbonate (DMC) solvent, and then dried for 20 minutes. Then, eight sheets were packed in a gold O-ring
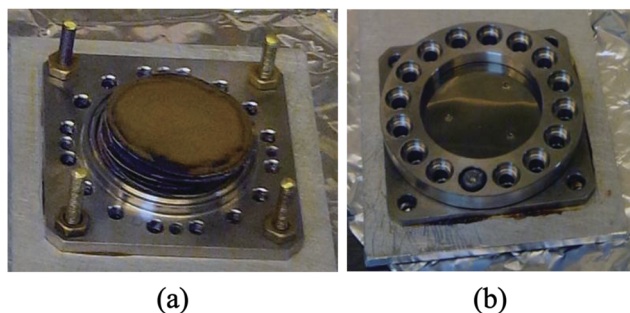

Fig. 4 Photographs of (a) the C_6Li sheets in the Ti cell and (b) the Ti cell with Ti foil window. Immediately before pumping the sample space, small holes were made on the Ti window so as to avoid an increase in the pressure in the cell.

sealed titanium (Ti) cell (see Fig. 4), because LIG is very sensitive to moisture in the air. The surface muons penetrate a Ti window with 50 μm thickness, but stop into the sheets with 82×8 μm thickness.

The μ$^+$SR experiments were performed on the EMU[17] surface muon beam line at ISIS of Rutherford Appleton Laboratory in U.K. In order to know a small change in an internal nuclear magnetic field due to Li-diffusion, the μ$^+$SR spectra were measured in zero field (ZF), a weak longitudinal field (LF), and a weak transverse field (wTF) in the temperature (T) range between 50 and 500 K using a cryo-oven. The sample in the Ti-cell was mounted on the Cu holder of the cryo-oven, which is cooled down to around 10 K with a closed cycle refrigerator and heated up to around 600 K without setup change.

μ$^+$SR is a common technique for investigating magnetic properties in solids through a direct measurement of an internal magnetic field (H_{int}), particularly in condensed matter physics.[18,19] Recently, μ$^+$SR also becomes popular in materials science,[6,20,21] because ion diffusion in solids was detected with μ$^+$SR from a small deviation of H_{int} caused by a dynamic behavior of ions.[6,10,12,22–25] More correctly, H_{int} is observed through the muon spin depolarization function of time [$P(t)$]. Here, the initial muon spin at $t = 0$ is perfectly antiparallel to its momentum due to parity violation of weak interaction, i.e. $P(0) = 1$. $P(t)$ is obtained by counting a number of decay positrons (e$^+$) using scintillation counters, because e$^+$ is emitted preferably along the direction of the muon spin, when the muon decays. The experimental technique of μ$^+$SR is described elsewhere.[18,19] The detailed explanation how to detect ion diffusion in solids with μ$^+$SR is given elsewhere.[6,10,12]

The implanted muons naturally stop both in LIG and the Cu collector in our arrangement mentioned above. Since the fraction of the implanted muons stopped in each phase of a sample is proportional to a volume fraction of each phase, a μ$^+$SR spectrum provides mainly two components corresponding to LIG and the Cu collector. Thus, the μ$^+$SR spectra for the Cu foil were also measured using the same setup as that for the LIG sheet, while twelve Cu foil sheets were placed into the Ti-cell.

3 Results

3.1 C_6Li

Fig. 5(a) shows the ZF- and LF-μ$^+$SR time spectra for the C_6Li sheets recorded at 50 K. The spectra clearly indicate that the internal magnetic field (H_{int}) detected by μ$^+$ is static. Since the applied LF = 10 Oe (= 10 000/4π A m^{-1}) significantly suppresses a relaxation due to H_{int},[26] the magnitude of H_{int} ranges around 10 Oe and matches the nuclear magnetic field mainly caused by the nuclear moments of ^6Li, ^7Li, ^{63}Cu, and ^{65}Cu. However, the ZF-μ$^+$SR spectrum becomes dynamic with increasing temperature and finally exhibits a small relaxation at 370 K [see Fig. 5(b)]. This means that the distribution of H_{int} becomes homogeneous at high temperatures due to Li-diffusion, as in the case for the other electrode materials.

In order to extract H_{int} in LIG, the ZF- and LF-μ$^+$SR spectra of the sheet were fitted by a combination of two dynamic Gaussian Kubo-Toyabe (KT) functions (G^{DGKT})[27] and a time-independent
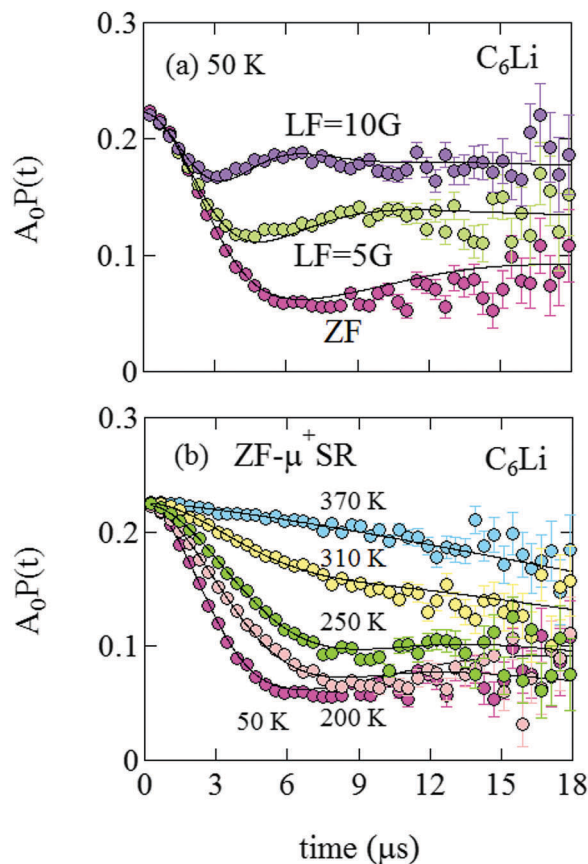
Fig. 5 (a) ZF- and LF-μ^+SR time spectra for C_6Li measured at 50 K. The magnitude of LF was 5 and 10 Oe. (b) The temperature variation of the ZF-μ^+SR spectrum from 50 to 370 K.

offset signal. Here, the two KT components correspond to the signals from C_6Li and the Cu foil, and the offset component comes from the muons stopped in the Ti-cell;

$$A_0P(t) = A_{C_6Li}G^{DGKT}(\Delta_{C_6Li}, \nu_{C_6Li}, t) + A_{Cu}G^{DGKT}(\Delta_{Cu}, \nu_{Cu}, t) + A_{BG}. \tag{1}$$

Here, A_0 is the initial ($t = 0$) asymmetry, A_{C_6Li}, A_{Cu}, and A_{BG} are the asymmetries for the muons stopped in C_6Li, Cu foil, and the powder cell. Δ is the static width of the local field distribution at the disordered sites, ν is the field fluctuation rate.

Fig. 6 shows the temperature dependences of Δ_{Cu} and ν_{Cu} estimated by fitting the ZF- and LF-μ^+SR spectra for the Cu foil with eqn (1) but $A_{C_6Li} = 0$. Both the $\Delta_{Cu}(T)$ and $\nu_{Cu}(T)$ curves exhibit a typical μ^+ diffusion behavior in a metal, in which μ^+ does not make a stable bond with negative ions, above around 125 K. That is, as temperature increases from 50 K, Δ_{Cu}, which corresponds to a spin–spin relaxation rate ($1/T_2$), is temperature independent up to around 125 K, and then starts to decrease with further increasing temperature, and finally becomes almost 0 above around 300 K. Such behavior is well known as a motional narrowing. Also, ν_{Cu}, which corresponds to a spin–lattice relaxation rate ($1/T_1$), increases with increasing temperature, and reaches a maximum at around 200 K, then rapidly decreases with further increasing temperature, and becomes 0 above 350 K. Here, ν_{Cu} indicates the hopping rate
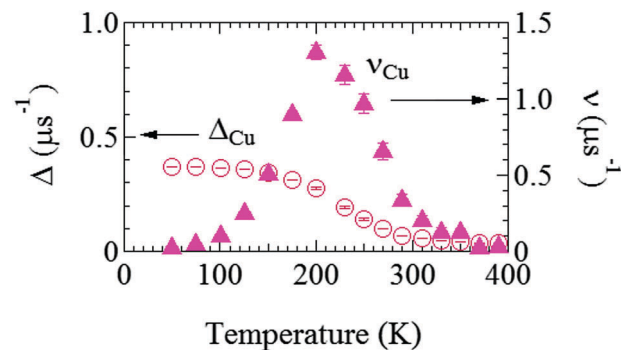

Fig. 6 The temperature dependences of field distribution width (Δ_{Cu}) (left) and field fluctuation rate (ν_{Cu}) (right) of the Cu foil. The data were obtained by fitting the μ^+SR spectra for the Cu foil with eqn (1) but $A_{C_6Li} = 0$.

of μ^+, and above 200 K, the hopping rate is too fast to be detected by μ^+SR. Although this muon diffusion can be also described by the behavior of the fixed Δ and increasing ν,[49] we dared not to fix Δ in order to exhibit that the internal magnetic field due to the nuclear magnetic moments of Cu seems to decrease with increasing temperature from diffusing muons.

Using these values for the A_{Cu} signal in the C_6Li sheet, both Δ_{C_6Li} and ν_{C_6Li} were successfully determined at each temperature with common A_{C_6Li}, A_{Cu}, and A_{BG}, namely, $A_{C_6Li} = 0.111(2)$, $A_{Cu} = 0.068(2)$, and $A_{BG} = 0.041(1)$. Since A_i is roughly proportional to the volume fraction (V_F) of i-th phase, V_F of C_6Li is estimated as 58% and that of Cu as 42% in the anode sheet. Such estimation is comparable with V_F calculated from the thickness of the graphite layer and Cu foil in the sheet, that is, 53% and 47%.

Fig. 7(a) and (b) show the temperature dependences of Δ_{C_6Li} and ν_{C_6Li}, which also exhibit a motional narrowing behavior above $\sim$230 K. The origin of such behavior is naturally thought to be either μ^+ diffusion or Li^+ diffusion. Note that very similar behavior was also reported with the past ZF-μ^+SR measurements on C_6Li.[28] Furthermore, since Li-NMR shows a motional narrowing behavior above $\sim$240 K,[11] the diffusive behavior detected with μ^+SR is most likely caused by Li-diffusion. In fact, first principles calculations predicts that the implanted μ^+ makes a bond with C, and as a result, μ^+ is more stable than Li^+ in the C_6Li lattice, as described later.

3.2 $C_{12}Li$

Fig. 8(a) shows the ZF- and LF-μ^+SR spectra for the $C_{12}Li$ sheets recorded at 50 K. The spectra also indicate a KT type relaxation caused by the nuclear moments of Li and Cu, as in the case for C_6Li. The temperature variation of the ZF-μ^+SR spectrum is similar to C_6Li (Fig. 5) too. However, in order to fit these spectra, we need an additional KT signal, i.e.

$$\begin{aligned} A_0P(t) &= A^1_{C_{12}Li}G^{DGKT}(\Delta^1_{C_{12}Li}, \nu_{C_{12}Li}, t) \\ &+ A^2_{C_{12}Li}G^{DGKT}(\Delta^2_{C_{12}Li}, \nu_{C_{12}Li}, t) \\ &+ A_{Cu}G^{DGKT}(\Delta_{Cu}, \nu_{Cu}, t) + A_{BG}, \end{aligned} \tag{2}$$

where $A^i_{C_{12}Li}$ and $\Delta^i_{C_{12}Li}$ ($i = 1, 2$) are asymmetries and field distribution width for the two KT signals. Note that the $\nu_{C_{12}Li}$ is
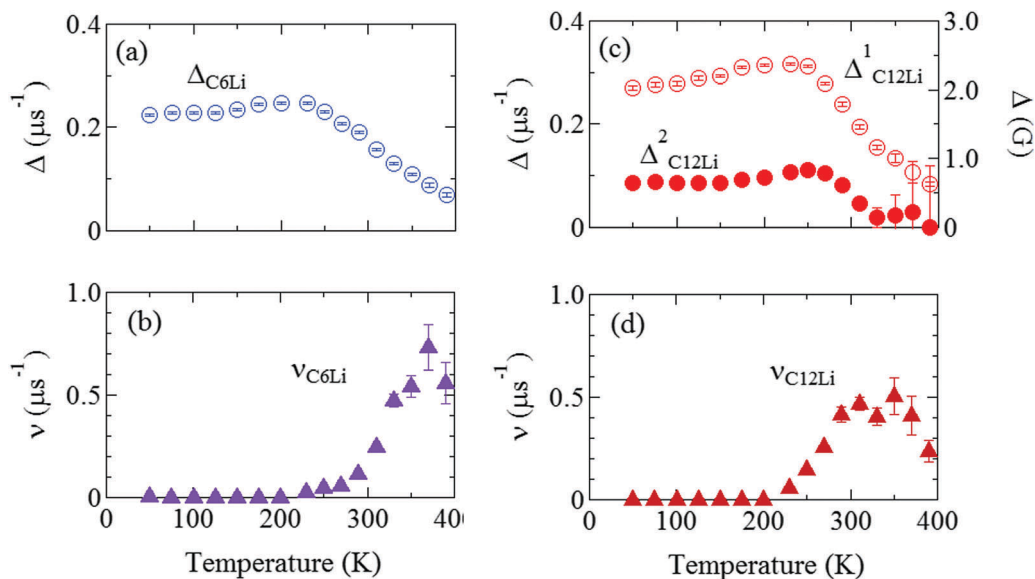
Fig. 7 The temperature dependences of the μ^+SR parameters for C_6Li and $C_{12}Li$; (a) the field distribution width for C_6Li ($\varDelta_{C_6Li}$), (b) field fluctuation rate for C_6Li (ν_{C_6Li}), (c) field distribution widths for $C_{12}Li$ $\left(\varDelta^1_{C_{12}Li}, \varDelta^2_{C_{12}Li}\right)$, and (d) field fluctuation rate for $C_{12}Li$ ($\nu_{C_{12}Li}$). The data were obtained by fitting the μ^+SR spectra for C_6Li with eqn (1) [for $C_{12}Li$ with eqn (2)].

common for the two $A_{C_{12}Li}$ signals. The fit provided that $A^1_{C_{12}Li}$ = 0.0399(4), $A^2_{C_{12}Li}$ = 0.0539(7), A_{Cu} = 0.0657(7), and A_{BG} = 0.0645, respectively. Thus, V_Fs of the two KT signals from $C_{12}Li$ were estimated as 25% and 34%, and that of Cu foil as 49% in the $C_{12}Li$ sheet. These values are also comparable with the calculated V_F, that is, 53% for graphite and 47% for Cu.

Fig. 7(c) and (d) show the temperature dependences of $\varDelta^i_{C_{12}Li}$ (i = 1, 2) and $\nu_{C_{12}Li}$ for $C_{12}Li$. As temperature increases from 50 K, both $\varDelta^i_{C_{12}Li}$ (i = 1, 2) are almost temperature independent (or slightly increases) up to 230 K, then they start to decrease above 250 K, and decrease monotonically with temperature. On the other hand, $\nu_{C_{12}Li}$ is eventually zero up to ∼230 K, but $\nu_{C_{12}Li}$ starts to increase further with increasing temperature, reaches a maximum around 350 K, and then decreases with further increasing temperature. This behavior is very similar to that of C_6Li, implying of the occurrence of Li diffusion above 230 K. Since $\varDelta^1_{C_{12}Li}$ (50 K) ∼ 3 × $\varDelta^2_{C_{12}Li}$ (50 K), the second muon site in the $C_{12}Li$ lattice is most to be likely far away from the Li layer.

It should be noted that $\varDelta^2_{C_{12}Li}$ (50 K) is almost equivalent to $\varDelta_{C_6Li}$ (50 K). This suggests that the local environment at μ^+ in C_6Li is very similar to that in $C_{12}Li$. It should be also emphasized that the number of muons implanted into the C_6Li ($C_{12}Li$) sample is so small (10^5 s^{-1})[29] that we can ignore the interaction between μ^+s.

4 Discussion

4.1 Muon site

Prior to the discussion of the Experimental data, we need to know the muon site(s) and situation in the C_6Li and $C_{12}Li$ lattices. First principles calculations based on density
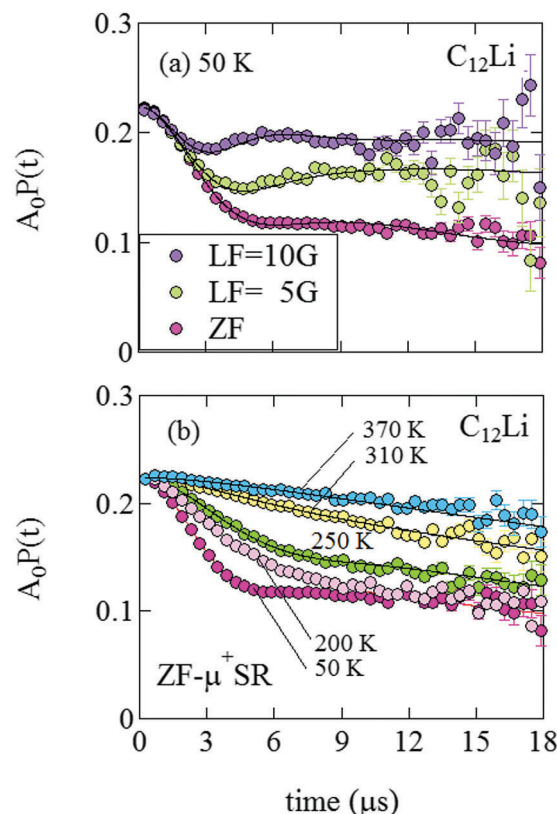

Fig. 8 (a) The ZF- and LF-μ^+SR time spectra for $C_{12}Li$ measured at 50 K. The magnitude of LF was 5 and 10 Oe. (b) The temperature variation of the ZF-μ^+SR spectrum from 50 to 370 K.

functional theory[30,31] revealed that the implanted μ^+ forms a stable bond with C in the graphene layer like a C–H bond with sp^3 orbital hybridization [Fig. 10(d)] and, as a result, sits at

19062 | *Phys. Chem. Chem. Phys.*, 2017, **19**, 19058–19066

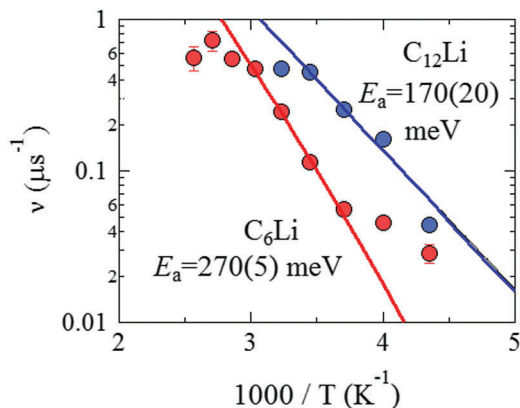This journal is © the Owner Societies 2017

Fig. 9 The relationship between ν and inverse temperature for C_6Li and $C_{12}Li$. The solid lines represent the best fit using eqn (3) with E_a = 270 ± 5 meV for C_6Li in the temperature range between 270 and 330 K and E_a = 170 ± 20 meV for $C_{12}Li$ in the temperature range between 230 and 290 K.

$\mu^1_{C_6Li}$ = (0.35, 0.37, 0.08). The same calculations for $C_{12}Li$ indicated that there are two stable muon sites, namely, at $\mu^1_{C_{12}Li}$ = (0.37, 0.37, 0.04) in the Li layer and at $\mu^2_{C_{12}Li}$ = (0.67, 0.66, 0.47) in the graphene layer. μ^+s at both sites also form a stable C–μ bond [Fig. 10(e) and (f)], as in C_6Li.

Details of the calculations are described in Appendix. Consequently, these results demonstrate that μ^+ is more stable than Li^+ in both C_6Li and $C_{12}Li$ lattice and support that the extracted ν from the μ^+SR data corresponds to the hopping rate of Li^+.

The predicted muon sites and Δ, which was given by dipole field calculations with DipElec,[32] are summarized in Table 2.

It is found that the calculated results are qualitatively consistent with the experimental results. Note that, since the dipole field calculations provide Δ^{cal} at 0 K without thermal vibration, Δ^{cal} is usually larger than Δ^{mea}.[33] The fact that $\Delta^{cal} \sim 2/3\Delta^{mea}$ only for $\mu^2_{C_{12}Li}$ would imply either an insufficient accuracy of the DFT calculations, a limited time window of μ^+SR, or the presence of imperfection in the samples. For the second factor, if $\Delta < 0.65$ Oe, we need to measure the μ^+SR spectrum until 25 μs to estimate Δ. However, such measurements are eventually impossible due to a lifetime of μ (~ 2.2 μs).

4.2 Temperature dependence of ν

In order to compare ν for C_6Li with that for $C_{12}Li$, Fig. 9 shows ν_{C_6Li} and $\nu_{C_{12}Li}$ as a function of inverse temperature ($1/T$). When ν is caused by Li-diffusion, a thermal activation process is naturally applicable for explaining the temperature dependence, *i.e.*

$$\nu = \nu_0 \exp(-E_a/k_BT) + \nu_{BG}, \qquad (3)$$

where ν_0 is the frequency factor, E_a is the activation energy, k_B is the Boltzmann's constant, and ν_{BG} is the temperature-independent ν.

From the linear relationship between $\log(\nu)$ and $1/T$, E_a is estimated as 270(5) meV for C_6Li in the T range between 270 and 310 K and 170(20) meV for $C_{12}Li$ in the T range between 230 and 290 K. Such a difference in E_a is probably caused by the strength of an interlayer interaction with Li^+ ions in the adjacent Li layers.
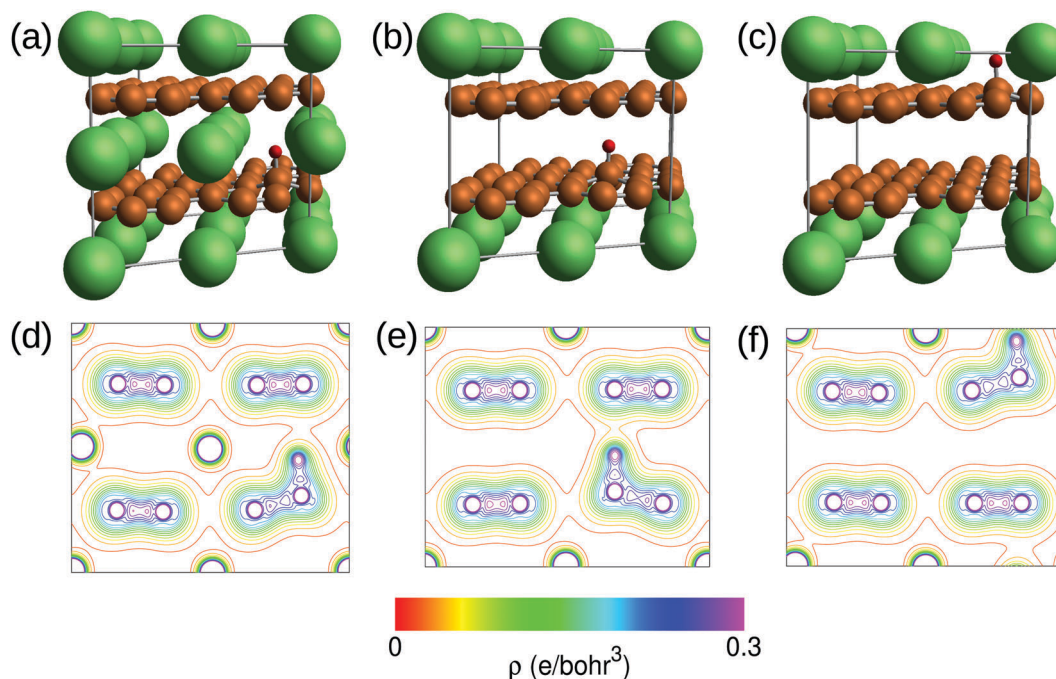

Fig. 10 Illustrations of the structures optimized by the calculations of (a) μ^+ in C_6Li, (b) μ^+ in the graphene layer and (c) in the Li layer of $C_{12}Li$. (d–f) The charge contour plots in the (110) plane corresponding to these optimized structures (a–c). The contour spacing is 0.02 e Bohr^{-3}. The lines for the densities higher than 0.3 e Bohr^{-3} are omitted.

This journal is © the Owner Societies 2017

Phys. Chem. Chem. Phys., 2017, **19**, 19058–19066 | **19063**

Table 2 The muon site in the Li-intercalated graphites predicted by first principles calculations and the field distribution width (Δ) at the muon site estimated by dipole field calculations and measured at 50 K

Compound	Site name	Coordinate (x, y, z)	$d_{\mu-\text{Li}}$ (Å)	Calculated Δ		Measured Δ at 50 K	
				(Oe)	(μs^{-1})	(Oe)	(μs^{-1})
$C_6\text{Li}$	$\mu^1_{C_6\text{Li}}$	(0.35, 0.35, 0.08)	1.51	4.16	0.354	2.61(9)	0.223(2)
$C_{12}\text{Li}$	$\mu^1_{C_{12}\text{Li}}$	(0.37, 0.37, 0.04)	3.96	4.14	0.353	3.17(1)	0.270(4)
	$\mu^2_{C_{12}\text{Li}}$	(0.67, 0.66, 0.47)	1.61	0.65	0.055	1.01(0)	0.086(2)
	$\Delta^1_{C_{12}\text{Li}}/\Delta^2_{C_{12}\text{Li}}$		6.38			3.15	
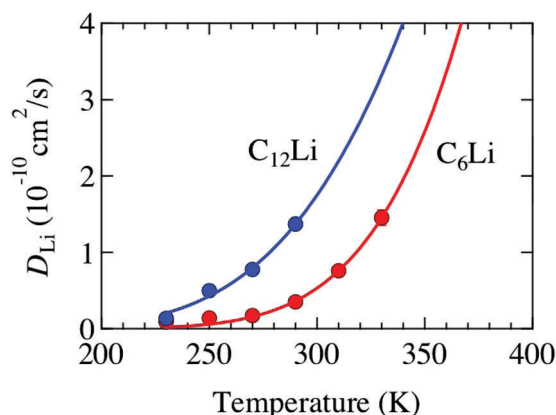
Fig. 11 The temperature dependence of the diffusion coefficient (D_{Li}) for $C_6\text{Li}$ and $C_{12}\text{Li}$. Solid lines represent the estimate from eqn (3) and (4).

4.3 Temperature dependence of Δ

As described in Sections 3.1 and 3.2, $\Delta_{C_6\text{Li}}$ and $\Delta_{C_{12}\text{Li}}$ are roughly temperature independent below 230 K, at which Li^+ ions are static. More correctly, as temperature increases from 50 to 200 K, both $\Delta_{C_6\text{Li}}$ and $\Delta^1_{C_{12}\text{Li}}$ increase by about 15%, for reasons currently unknown. Note that graphite[34,35] and alkali-metal intercalated graphites[36] exhibit negative thermal expansion

along the ab-plane (α_a) below room temperature and α_a ranges between -1 and -4×10^{-6} K^{-1}. The reduction of the distance between μ^+ and Li^+ is naturally expected to increase Δ. However, the effect of such negative thermal expansion on Δ was estimated as 0.1% over 200 K, which is too small to explain the experimental result ($\sim$15%).

In order to further discuss the temperature dependence of Δ below 230 K, we need to know the detailed displacement of the intercalated Li with temperature.

4.4 Diffusion coefficient of Li^+

Assuming that Li^+ diffuses through interstitial sites in the Li layer, the self diffusion coefficient (D_{Li}) is given by[37]

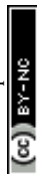$$D_{\text{Li}} = \sum_i \frac{1}{N_i} s_i^2 Z_{v,i} \nu, \tag{4}$$

where N_i, s_i, and $Z_{v,i}$ are the number of Li sites in the i-th diffusive path, the distance of the path, and vacancy fraction, respectively. Since one Li^+ ion in the Li layer is surrounded six vacant Li sites for a path to jump to the next vacant sites, $N_1 = 6$, $s_1 = 2 \times \frac{\sqrt{3}}{2} \times \frac{4.29}{3} = 2.48$ Å ($= 2.48 \times 10^{-10}$ m), and $Z_{v,i} = 1$. Therefore, we obtain that $D^{\mu\text{SR}}_{\text{Li}} = 7.6 \times 10^{-11}$ (cm^2 s^{-1}) for $C_6\text{Li}$ and $D^{\mu\text{SR}}_{\text{Li}} = 1.5 \times 10^{-10}$ (cm^2 s^{-1}) for $C_{12}\text{Li}$ at 310 K (Fig. 11).

Table 3 The diffusive coefficient D_{Li} around room temperature and E_a in Li intercalated graphite estimated with different techniques. D_{Li} represents a self diffusion coefficient, *i.e.* a jump diffusion coefficient, while $\tilde{D}_{\text{Li}}$ represents a chemical diffusion coefficient

	$C_6\text{Li}$		
	D_{Li} (cm^2 s^{-1})	$\tilde{D}_{\text{Li}}$ (cm^2 s^{-1})	E_a (meV)
μ^+SR (at 310 K)	$7.6(3) \times 10^{-11}$	—	270(5)
Li-NMR[11] (at 314 K)	3.8×10^{-11}	—	550
Li-NMR[44] (at 373 K)	10^{-8}	—	—
Electrochemical impedance[38] (at 298 K)	10^{-8}–10^{-7}	—	—
First principles calculations[42] (at 300 K)	0.9×10^{-11}	—	283
First principles calculations[45] (at 300 K)	—	1–10×10^{-11}	510

	$C_{12}\text{Li}$		
	D_{Li} (cm^2 s^{-1})	$\tilde{D}_{\text{Li}}$ (cm^2 s^{-1})	E_a (meV)
μ^+SR (at 310 K)	$14.6(4) \times 10^{-11}$	—	170(20)
Li-NMR[44] (at 373 K)	2.4×10^{-7}	—	—
Electrochemical impedance[38] (at 298 K)	5.3×10^{-7}	—	—
PITT[39] (at 328 K)	—	0.01×10^{-11}	—
Current pulse relaxation[40] (at 300 K)	—	0.8×10^{-11}	—
Potential step chronoamperometry[40] (at 300 K)	—	0.1×10^{-11}	—
First principles calculations[42] (at 300 K)	0.9×10^{-11}	—	297

19064 | *Phys. Chem. Chem. Phys.*, 2017, **19**, 19058–19066

This journal is © the Owner Societies 2017

Then, we discuss the reliability of D_{Li} estimated with μ$^+$SR. Table 3 lists several D_{Li} for C_6Li and $C_{12}Li$ reported with different techniques. The present μ$^+$SR showed that D_{Li} for C_6Li and $C_{12}Li$ ranges in the order of 10^{-11}–10^{-10} cm^2 s^{-1} and D_{Li} for C_6Li is slightly smaller than D_{Li} for $C_{12}Li$. This is very consistent with $D_{Li}(C_6Li)$ determined by the recent Li-NMR measurements, i.e. $D_{Li}^{NMR} = 3.8 \times 10^{-11}$ (cm^2 s^{-1}) at 314 K.[11] Also, $D_{Li}^{\mu SR}$ is comparable to D_{Li} predicted by first principles calculations. Furthermore, the past NMR[11] and electrochemical measurements[38–40] are likely to support the present result, i.e. $D_{Li}(C_6Li) < D_{Li}(C_{12}Li)$, although the latter provided not D_{Li} but a chemical diffusion coefficient ($\tilde{D}_{Li}$).

In a highly oriented graphite (HOPG), D_{Li} for C_6Li and $C_{12}Li$ in the direction parallel/perpendicular to the graphene layer is also reported as $\tilde{D}_{Li}^{//} \sim 10^{-7}$–$10^{-6}$ cm^2 s^{-1} and $\tilde{D}_{Li}^{\perp} \sim 10^{-11}$ cm^2 s^{-1}, respectively.[41] If we assume the relation $\tilde{D}_{Li} = \Theta D_{Li}$, where thermodynamic factor $\Theta(x) = 10^3$–10^4 for C_6Li and $C_{12}Li$,[42] $D_{Li}^{//}$ is similar to $D_{Li}^{\mu SR}$. This shows that μ$^+$SR "sees" Li diffusion in graphene layer. Such anisotropic diffusion in layered materials could be detected separately with μ$^+$SR in the future, based on a theoretical prediction of H_{int} in a low dimensional system.[43]

Concerning the thermal activation energy (E_a), the present μ$^+$SR result is comparable to the NMR result and very consistent with the prediction from the calculations. In overall, μ$^+$SR is found to provide reasonable D_{Li} and to confirm that D_{Li} in LIG ranges in the same order to those for positive electrode materials.

5 Conclusions

We have observed Li diffusion in C_6Li and $C_{12}Li$ by μ$^+$SR using the discharged negative electrode sheet, which was prepared by coating a graphite layer onto a Cu foil. Li diffusion was clearly detected with μ$^+$SR through a small deviation of H_{int} caused by Li diffusion. A diffusion coefficient of Li (D_{Li}) in C_6Li and $C_{12}Li$ was found to range in the same order of D_{Li} in positive electrode materials, that is, 10^{-10} (cm^2 s^{-1}) at room temperature. The thermal activation energy (E_a) of D_{Li} was estimated as 270(5) meV for C_6Li and 170(20) meV for $C_{12}Li$. These values are comparable with those obtained by Li-NMR[11] and predicted by first principles calculations.[42] The difference of E_a between C_6Li and $C_{12}Li$ is probably due to an interlayer electrostatic interaction from the adjacent Li layers. Since the Li diffusion in the anode sheet has been clarified by μ$^+$SR, it is ready to measure Li diffusion in a Li-ion battery in an in operando manner.

Appendix: muon sites

The first-principles calculations based on density functional theory[30,31] have been performed to determine the muon site in C_6Li and $C_{12}Li$. The ultrasoft pseudopotential method[46,47] is used and the generalized gradient approximation[48] is adopted for the exchange–correlation energy. The position of μ$^+$ is simulated using a hydrogen pseudopotential, where a deficient electron is compensated by the uniform background charge. The Li-1s state is treated as the valence. The calculations are carried out with the $2 \times 2 \times 2$ supercell for C_6Li and $2 \times 2 \times 1$ for $C_{12}Li$. The $4 \times 4 \times 4$ k-point mesh is used for the Brillouin zone integration. For $C_{12}Li$, both cases of μ$^+$ being in the graphene layer and in the Li layer are considered. In the structural optimization process, the lattice constants are fixed at the experimental values and the atom positions are fully relaxed without any symmetry restrictions. The initial μ$^+$ position is set to be about 1.4 Å above the center of the C–C bond. The results of the structural optimization are summarized in Fig. 10. In all cases, the μ$^+$ positions are the on-top site on the C layer as shown in Fig. 10(a)–(c). The charge contour plots given in Fig. 10(d)–(f) indicate clear evidence of the C–μ$^+$ bond formation which pulls up the C atom from the layer. The C atom is most likely stabilized by constructing sp^3 hybrids. When the μ$^+$ is located in the Li layer, the C–μ$^+$ bond is slightly tilted due to an adjacent Li atom. The C–μ$^+$ bond lengths are 1.13–1.14 Å which are close to typical C–H ones of ca. 1.1 Å. Because of the existence of the C–μ$^+$ bond, the μ$^+$ is expected to be immobile in C_6Li and $C_{12}Li$.

References

1 D. D. L. Chung, J. Mater. Sci., 2002, 37, 1475–1489.
2 V. Etacheri, R. Marom, R. Elazari, G. Salitra and D. Aurbach, Energy Environ. Sci., 2011, 4, 3243–3262.
3 K. Momma and F. Izumi, J. Appl. Crystallogr., 2011, 44, 1272–1276.
4 Y. X. Zhao and I. L. Spain, Phys. Rev. B: Condens. Matter Mater. Phys., 1989, 40, 993–997.
5 R. Juza and V. Wehle, Naturwissenschaften, 1965, 52, 537.
6 J. Sugiyama, K. Mukai, Y. Ikedo, H. Nozaki, M. Månsson and I. Watanabe, Phys. Rev. Lett., 2009, 103, 147601.
7 J. Sugiyama, Y. Ikedo, K. Mukai, H. Nozaki, M. Månsson, O. Ofer, M. Harada, K. Kamazawa, Y. Miyake, J. H. Brewer, E. J. Ansaldo, K. H. Chow, I. Watanabe and T. Ohzuku, Phys. Rev. B: Condens. Matter Mater. Phys., 2010, 82, 224412.
8 J. Sugiyama, H. Nozaki, M. Harada, K. Kamazawa, O. Ofer, M. Månsson, J. H. Brewer, E. J. Ansaldo, K. H. Chow, Y. Ikedo, Y. Miyake, K. Ohishi, I. Watanabe, G. Kobayashi and R. Kanno, Phys. Rev. B: Condens. Matter Mater. Phys., 2011, 84, 054430.
9 J. Sugiyama, H. Nozaki, M. Harada, K. Kamazawa, Y. Ikedo, Y. Miyake, O. Ofer, M. Månsson, E. J. Ansaldo, K. H. Chow,

This journal is © the Owner Societies 2017

Phys. Chem. Chem. Phys., 2017, 19, 19058–19066 | 19065

G. Kobayashi and R. Kanno, *Phys. Rev. B: Condens. Matter Mater. Phys.*, 2012, **85**, 054111.

10 J. Sugiyama, K. Mukai, M. Harada, H. Nozaki, K. Miwa, T. Shiotsuki, Y. Shindo, S. R. Giblin and J. Lord, *Phys. Chem. Chem. Phys.*, 2013, **15**, 10402–10412.

11 J. Langer, V. Epp, P. Heitjans, F. A. Mautner and M. Wilkening, *Phys. Rev. B: Condens. Matter Mater. Phys.*, 2013, **88**, 094304.

12 M. Mansson and J. Sugiyama, *Phys. Scr.*, 2013, **88**, 068509.

13 J. Sugiyama, K. Mukai, H. Nozaki, M. Harada, M. Månsson, K. Kamazawa, D. Andreica, A. Amato and A. D. Hillier, *Phys. Rev. B: Condens. Matter Mater. Phys.*, 2013, **87**, 024409.

14 S. Klamor, K. Zick, T. Oerther, F. M. Schappacher, M. Winter and G. Brunklaus, *Phys. Chem. Chem. Phys.*, 2015, **17**, 4458–4465.

15 S. Taminato, M. Yonemura, S. Shiotani, T. Kamiyama, S. Torii, M. Nagao, Y. Ihikawa, K. Mori, T. Fukunaga, Y. Onodera, T. Naka, M. Morishima, Y. Ukyo, D. S. Adipranoto, H. Arai, Y. Uchimoto, Z. Ogumi, K. Suzuki, M. Hirayama and R. Kanno, *Sci. Rep.*, 2016, **6**, 28843.

16 https://www.srim.org.

17 S. Giblin, S. Cottrell, P. King, S. Tomlinson, S. Jago, L. Randall, M. Roberts, J. Norris, S. Howarth, Q. Mutamba, N. Rhodes and F. Akeroyd, *Nucl. Instrum. Methods Phys. Res., Sect. A*, 2014, **751**, 70.

18 G. M. Kalvius, D. R. Noakes and O. Hartmann, in *Handbook on the Physics and Chemistry of Rare Earths*, ed. K. A. Gschneidner, J. L. Eyring and G. H. Lander, North-Holland, Amsterdam, 2001, vol. 32, ch. 206, pp. 55–451.

19 A. Yaouanc and P. D. de Reotier, *Muon Spin Rotation, Relaxation, and Resonance: Applications to Condensed Matter*, Oxford, Oxford, 2011.

20 R. Mashita, H. Kishimoto, R. Inoue, A. Koda, R. Kadono and T. Kanaya, *Polymer*, 2016, **105**, 510–515.

21 A. D. Pant, Y. Sugawara, I. Yanagihara, G. P. Khanal, I. Shiraki, W. Higemoto, K. Shimomura, K. Ishida, F. L. Pratt, E. Torikai and K. Nagamine, *J. Phys. Soc. Conf. Proc.*, 2015, **8**, 033007.

22 A. S. Powell, J. S. Lord, D. H. Gregory and J. J. Titman, *J. Phys. Chem. C*, 2009, **113**, 20758–20763.

23 A. S. Powell, Z. Stoeva, J. S. Lord, R. I. Smith, D. H. Gregory and J. J. Titman, *Phys. Chem. Chem. Phys.*, 2013, **15**, 816–823.

24 T. E. Ashton, J. V. Laveda, D. A. MacLaren, P. J. Baker, A. Porch, M. O. Jones and S. A. Corr, *J. Mater. Chem. A*, 2014, **2**, 6238–6245.

25 M. Amores, T. E. Ashton, P. J. Baker, E. J. Cussen and S. A. Corr, *J. Mater. Chem. A*, 2016, **4**, 1729–1736.

26 R. S. Hayano, Y. J. Uemura, J. Imazato, N. Nishida, T. Yamazaki and R. Kubo, *Phys. Rev. B: Condens. Matter Mater. Phys.*, 1979, **20**, 850–859.

27 R. Kubo and T. Toyabe, in *Magnetic Resonance and Relaxation*, ed. R. Bline, North-Holland, Amsterdam, 1996.

28 J. A. Chakhalian, R. F. Kiefl, S. R. Dunsiger, W. A. MacFarlane, R. Miller, J. E. Sonier and J. E. Fischer, *Phys. Rev. B: Condens. Matter Mater. Phys.*, 2002, **66**, 155107.

29 http://www.isis.ral.ac.uk.

30 P. Hohenberg and W. Kohn, *Phys. Rev.*, 1964, **136**, B864.

31 W. Kohn and L. Sham, *Phys. Rev.*, 1965, **140**, A1133.

32 K. M. Kojima, J. Yamanobe, H. Eisaki, S. Uchida, Y. Fudamoto, I. M. Gat, M. I. Larkin, A. Savici, Y. J. Uemura, P. P. Kyriakou, M. T. Rovers and G. M. Luke, *Phys. Rev. B: Condens. Matter Mater. Phys.*, 2004, **70**, 094402.

33 J. Sugiyama, H. Nozaki, K. Mukai, M. Harada, M. Mansson and A. Hillier, *Solid State Ionics*, 2014, **262**, 901–903.

34 D. Tsang, B. Marsden, S. Fok and G. Hall, *Carbon*, 2005, **43**, 2902–2906.

35 J. B. Nelson and D. P. Riley, *Proc. Phys. Soc.*, 1945, **57**, 477.

36 S. E. Hardcastle and H. Zabel, *Phys. Rev. B: Condens. Matter Mater. Phys.*, 1983, **27**, 6363–6369.

37 R. J. Borg and G. J. Dienes, *An Introduction to Solid State Diffusion*, Academic Press, San Diego, 1988, ch. 3, pp. 53–77.

38 A. Funabiki, M. Inaba, Z. Ogumi, S. Yuasa, J. Otsuji and A. Tasaka, *J. Electrochem. Soc.*, 1998, **145**, 172–178.

39 P. Yu, B. N. Popov, J. A. Ritter and R. E. White, *J. Electrochem. Soc.*, 1999, **146**, 8–14.

40 T. Uchida, Y. Morikawa, H. Ikuta, M. Wakihara and K. Suzuki, *J. Electrochem. Soc.*, 1996, **143**, 2606–2610.

41 K. Persson, V. A. Sethuraman, L. J. Hardwick, Y. Hinuma, Y. S. Meng, A. van der Ven, V. Srinivasan, R. Kostecki and G. Ceder, *J. Phys. Lett.*, 2010, **1**, 1176–1180.

42 K. Persson, Y. Hinuma, Y. S. Meng, A. Van der Ven and G. Ceder, *Phys. Rev. B: Condens. Matter Mater. Phys.*, 2010, **82**, 125416.

43 G. Solt, *Hyperfine Interact.*, 1995, **96**, 167–175.

44 Y. Saito, H. Kataoka, K. Nakai, J. Suzuki, K. Sekine and T. Takamura, *J. Phys. Chem. B*, 2004, **108**, 4008–4012.

45 K. Toyoura, Y. Koyama, A. Kuwabara, F. Oba and I. Tanaka, *Phys. Rev. B: Condens. Matter Mater. Phys.*, 2008, **78**, 214303.

46 D. Vanderbilt, *Phys. Rev. B: Condens. Matter Mater. Phys.*, 1990, **41**, 7892.

47 K. Miwa, *Phys. Rev. B: Condens. Matter Mater. Phys.*, 2011, **84**, 094304.

48 K. B. J. P. Perdew and M. Ernzerho, *Phys. Rev. Lett.*, 1996, **77**, 3865.

49 H. Schilling, M. Camani, F. N. Gygax, W. Ruegg and A. Schenck, *J. Phys. F: Met. Phys.*, 1982, **12**, 875.

19066 | *Phys. Chem. Chem. Phys.*, 2017, **19**, 19058–19066

This journal is © the Owner Societies 2017